Theor Chem Acc (2001) 105:309–322
DOI 10.1007/s002140000218

Theoretical
Chemistry Accounts

Regular article

Direct-space analysis of the Si–Si bonding pattern in the π-bonded chain reconstructed Si(111)(2 × 1) surface

F. Cargnoni[1], **C. Gatti**[2]

[1] Dipartimento di Chimica Fisica ed Electrochimica, Università di Milano, via Golgi 19, 20133 Milan, Italy
[2] Centro CNR per lo Studio delle Relazioni tra Struttura e Reattività Chimica, via Golgi 19, 20133 Milan, Italy

Received: 19 July 2000 / Accepted: 2 October 2000 / Published online: 23 January 2001
© Springer-Verlag 2001

Abstract. Atomic and bond properties of silicon atoms in the buckled π-bonded chain reconstructed Si(111)(2 × 1) system were investigated by applying the quantum theory of atoms in molecules to a number of wavefunctions from periodic ab initio calculations using a slab model for the surface and geometries from experiment. Reconstruction involves much larger surface-cell charge distortions than in the unrelaxed surface and drastic changes in the atomic polarizations of the surface layer atoms. The effect of buckling is to largely differentiate the properties (charge, energy, volume, atomic polarizations) of the two unique atoms of each surface layer. The direction of electronic charge transfer in the topmost chain (from the "up" to the "down" atom) was found to be opposite to what was claimed previously. The π conjugation is not strictly localized along the topmost layer chains (where it is also largely incomplete), but rather it extends over a 2D array of bonds between the topmost and the lower surface layers.

Key words: Silicon surface reconstructions – First principles calculations – Electron density topology – Chemical bond – Surface-cell charge distortions

1 Introduction

One of the central issues of semiconductor surface physics is the reconstruction that the surface layers undergo with respect to the bulk structure [1–3]. Arising from the covalent character of bonding in most semiconductors, a very large change in the electronic structure may occur as a result of the bond breaking and reforming that quite often accompanies surface reconstruction. This change is of paramount importance since the electronic structure of semiconductor surfaces plays a crucial role in modern technology.

The Si(111) surface structure obtained after low-temperature ($T \leq 600$ K) ultrahigh vacuum cleavage and before annealing to higher temperatures exhibits a 2 × 1 low-energy electron diffraction (LEED) pattern [1–4]. This surface is a prototype of clean semiconductor surfaces and, although apparently simple, it has several intriguing features which have motivated almost 30 years of experimental and theoretical effort [1–3].

A basic key to understand the properties of this surface was provided by Pandey's proposal [5] of a structural model known as the π-bonded chain model, lately modified by several authors [6–16] by supplementing it with various degrees of buckling of the topmost layer chains. These improved models represent the lowest energy 2 × 1 reconstructions at different levels of theory [11–16] and, among the other structures proposed for such a system [3], they give overall best agreement with experiment; in particular with results from techniques that either probe the surface geometrical structure, like the quantitative LEED [7, 8, 10], the medium-energy ion scattering (MEIS) [9], or that investigate the surface electronic band features, like optical absorption [17], photoemission [18] and inverse photoemission [19], angle-resolved photoemission (ARPES) [18, 20], scanning tunneling microscopy [21] and spectroscopy [22], etc.

The π-bonded chain model involves an extensive displacement of the atoms in the surface layers, further bond breaking besides that due to cleaving, and rebonding. Namely, the reconstruction affords two layers of chain-bonded surface atoms: a top layer of threefold and a lower layer of fourfold coordinated atoms. The fundamental physical feature of the Pandey chain (PC) model is that the surface dangling bonds are on nearest neighbor sites rather than on next-nearest neighbor sites as in the (111)(1 × 1) surface; thus the zigzag chain of adjacent p_z orbitals can, in principle, π-bond as in organic materials, leading to the formation of bonding and antibonding surface π states and to the opening of a gap

Correspondence to: C. Gatti
e-mail: c.gatti@csrsrc.mi.enr.it

Contribution to the Proceedings of the 2000 Symposium on Chemical Bonding: State of the Art in Conceptual Quantum Chemistry

in the surface electronic structure as seen in photoemission experiments [18, 19]. A pronounced dispersion in both the valence and the conduction surface bands along the Γ-J direction of the 2D reciprocal lattice (the π-chain direction in real space) was also observed in the ARPES experiments [18, 20]. The ability of the PC model to reproduce such a dispersion has been a decisive factor in its support [1–3, 23]. A substantial buckling of the topmost layer chains ($b = 0.3$–0.5 Å) is then essential for a quantitative interpretation of most of the experimental results and it is also an unbiased outcome from the ab initio molecular dynamics simulation of the surface reconstruction [13] as well as from the other most recent theoretical approaches [11, 12, 15].

While there has been a great surge of interest in the surface electronic states of the Si(111)(2 × 1) surface, few studies [12, 14] have afforded the "chemical" features of this surface reconstruction.

Firstly, the nature of the bonding along the so-called π chain of the PC model deserves a closer inspection. Indeed π conjugation is expected to be rather unusual in the case of silicon, since no silicon analogues of benzene or graphite are actually known. The studies of Badziag and Verwoerd [12] and of Craig and Smith [14] considered the π bonding along the chains, using semiempirical cluster or slab calculations and orbital localization procedures for the bond analysis. Their conclusion was that the generally accepted assumption that atoms along the chains are π bonded needs revision and that there is also an important net electron transfer from the lowered to the raised chain atoms which seemingly counteracts π bonding. The direction of such charge transfer is, however, rather unexpected if one realizes that the lowered chain atom has a nearly planar sp^2 bonding arrangement, while the raised one shows an sp^3-like hybridization pattern. On the basis of purely energetic considerations one would expect an electron transfer in just the opposite direction to that claimed by Badziag and Verwoerd [12], Craig and Smith [14], and Ancillotto et al. [13].

Secondly, there are many other chemical features, following reconstruction, that call for further investigation. In fact, as prompted by Duke [1], the semiconductor surface structure should be appropriately visualized as a totally new 2D compound, epitaxially bonded to its bulk substrate, and exhibiting properties distinct from either the corresponding bulk solid or molecules based on the same atomic species. Of particular interest is the study of

1. The bonding properties and extent of π delocalization in both the topmost and lower layers of the surface.
2. The details of the overall charge transfer and energetic stabilization ensuing reconstruction.
3. The driving forces leading from the nonreconstructed Si(111)(1 × 1) surface to the (2 × 1) structure.

The aim of this article is, therefore, to provide a direct-space quantitative description and understanding of the Si (111)(2 × 1) surface reconstruction, as an effort to fill the gap of chemical knowledge on this system. A slab model for the surface, experimental geometries consistent with the PC model, and a fully periodic first principles approach is adopted in our calculations. As in our previous study of the Si (111)(1 × 1) and Si (111)(1 × 1)–H systems [24], the "chemical" information is derived by analyzing the computed wavefunctions in terms of the quantum theory of atoms in molecules (QTAM) [25]. This theory is firmly rooted in quantum mechanics, defines atomic subsystems whose properties are determined by physics and, in contrast to conventional methods of analysis, makes no use of any Hilbert space partitioning to extract information from wavefunctions. This fact appears as particularly welcome when dealing with homonuclear systems where – in spite of their being described by the same set of basis functions – large charge transfers among the atoms arise because of the quite different geometrical environment they experience. The ability of QTAM to deal with a quantitative analysis of the changes in bonding and atomic properties of Si in a variety of perturbed diamond-like Si lattices has been well documented [24, 26, 28]; namely, in the study of the self-interstitial clusters in silicon bulk [26], or of the bond-defect complexes also formed in Si bulk by the incomplete recombination of a vacancy–interstitial pair [27], or, finally, in the characterization of the properties of the first layer silicon atoms following surface formation and hydrogen adsorption on Si(111)(1 × 1) [24]. The use of QTAM should enable us to place the peculiar properties of the new 2D silicon compound, envisaged by Duke [1] and formed through the PC 2 × 1 surface reconstruction, on a quantitative basis. The bulk silicon and the ideal Si (111)(1 × 1) nonrelaxed surface are used as suitable reference systems in this work.

The article is organized as follows. Section 2 illustrates how we defined the slab models for the reconstructed surface and which computational procedures have been adopted. A brief survey of QTAM concepts used in the present work is also outlined. A thorough discussion of energetic results and of changes in the atomic and bonding properties ensuing the PC 2 × 1 surface reconstruction follows in Sect. 3. Comparisons and discrepancies with previous results are also highlighted and discussed there. Section 4 concludes.

2 Computational details

2.1 Hamiltonians

Calculations were performed using either the Hartree–Fock–Roothaan or the density functional Kohn–Sham fully periodic approaches, as implemented in the CRYSTAL98 code [29]. The local density approximation (LDA) [30], Becke's three parameter hybrid method with the Lee, Yang, and Parr correlation functional [31], or the Perdew–Wang generalized gradient approximation (PWGGA) correlation and exchange potentials [32] were tested in the density functional theory (DFT) computations. The use of restricted Hartree-Fock (RHF) and unrestricted Hartree–Fock (UHF) or of restricted and unrestricted DFT formalisms has allowed us to study either spin-nonpolarized or spin-polarized surfaces with antiferromagnetic or ferromagnetic spin alignments in the 2 × 1 unit cell. To force a spin-polarized solution the number of α and β electrons at all **k** points was locked [29] either for the first 20 self-consistent-field (SCF) cycles (antiferromagnetic case) or for at least the first 30 SCF cycles (ferromagnetic case), and then released. Ferromagnetic and antiferromagnetic solutions were started [29] by

computing the initial density matrix as the superposition of atomic densities and by assigning $\alpha\alpha$ or $\alpha\beta$ initial spin configurations to the two unique atoms of the topmost chain.

2.2 Basis sets

A 3-21G(d) type basis set was adopted [24, 33] using a fixed 0.6 exponent for the d function. The two scaling factors (SF) of the outermost *sp* shells were recursively optimized along with the cell parameter for the diamond structure of bulk silicon until their changes from cycle to cycle did not exceed 0.001 and 0.001 Å, respectively. Final adopted values for the reference bulk silicon and the reconstructed surface were 1.425 (inner valence shell SF), 1.390 (outer valence shell SF), and 5.475 Å (cell parameter) at the RHF level and 1.387, 1.354 and, 5.489 Å, respectively, at the DFT/PWGGA level. The experimental cell parameter is 5.431 Å [34].

2.3 Si(111)(2 × 1) surface model and geometry

A slab model for the surface and the related "SLAB" keyword in the CRYSTAL98 code were adopted. A slab is a 2D periodic structure, with two infinite periodic surfaces parallel to a chosen crystalline plane [in our case (111)] and a finite thickness [35]. We used a centrosymmetric slab, with a 2×1 unit cell and consisting of 14 layers, for a total of 28 Si atoms per cell. A ball-and-stick representation of the seven unique layers considered in our slab model for the PC reconstructed Si(111)(2 × 1) surface and the corresponding layers for the nonreconstructed Si(111)(1 × 1) surface is shown in Fig. 1. There is one unique atom (Si*N*L, $N = 1{,}7$) per layer in the nonreconstructed surface and two such atoms [Si($2N-1$) and Si($2N$), $N = 1{,}7$] in the reconstructed surface. Since a slab single-point calculation required about 40 h of computing time on a RISC machine of 20 SPECfp95 central processing unit peak performance, the global search of the equilibrium structure of the reconstructed surface was out of the reach of the computational approach adopted. More importantly, it was also beyond the scope of the present work. The atomic coordinates of the first 12 nonequivalent Si atoms in the Si(111)(2 × 1) surface were therefore taken from either LEED [7] or MEIS [9] structural analyses (both providing atomic positions down to the sixth layer), while those of the remaining two nonequivalent atoms were fixed at their bulk value. This choice ensures and assumes the presence of two central geometrically unperturbed layers of atoms in the adopted slab model. Finally, for each model Hamiltonian, the atomic coordinates were scaled so as to yield, for the short axis of the 2×1 unit cell, the same cell parameter as found for silicon bulk at the same level of theory. The final adopted geometries are hereinafter denoted as LEE or MEI to recall their derivation from LEED [7] and MEIS [9] analyses, respectively.

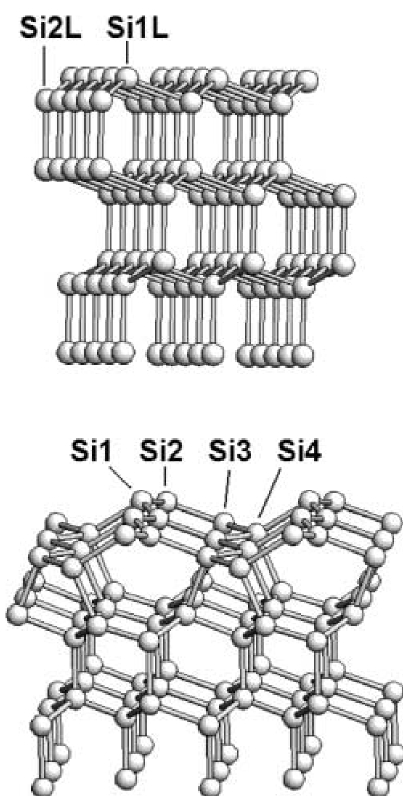

Fig. 1. Stick-and-ball representation and atomic numbering of: *top* the Si(111)(1 × 1) unrelaxed surface; *bottom* the Si(111)(2 × 1) reconstructed surface according to Pandey's π-bonded chain model [5] and the low-energy electron diffraction (*LEED*) geometry by Himpsel et al. [7]. Upon reconstruction, the surface dangling bonds are on nearest neighbor rather than on next-nearest neighbor sites

We note that the atomic positions from LEED or MEIS are not directly derived from experiment, rather they are in both cases the result of a model analysis that combines the available experimental outcomes with a Keating-like strain energy minimization [36, 37]. Subsurface relaxations and missing experimental information are taken into account in this way [7, 9].

At variance with MEIS determination [9] the LEED structure [7] exhibits an overall compression, as the outer chain moves 0.2 Å inward. However both analyses agree on a stronger buckling in the upper chain ($b = 0.38$ and 0.30 Å for LEED and MEIS, respectively) and a smaller one ($b = 0.07$ and 0.15 Å) in the lower chain, the b value being the absolute difference between the z coordinates of the two unique atoms of each layer and the z-axis being the surface normal. Significant buckling is also found in the succeeding three layers by both structural analyses. The amount of buckling in the outer chain estimated by the LEED analysis is close to the extreme case, where the down atom (Si2, Fig. 1) has a planar sp^2 bond configuration and, along with that found for the lower chain, it is much closer than MEIS estimates to the bucklings determined in a number of first principles investigations [13, 15, 16]. The latter studies used the local density functional approximation, a plane-wave basis set, and the related exploitation of the Hellmann–Feynman forces in the total-energy minimization [38].

2.4 Si(111)(1 × 1) surface model and geometry

For comparison purposes with the reconstructed surface, the nonrelaxed (NR) geometrical model of the Si(111)(1 × 1) slab was selected and defined as in Ref. [24]. Computations were done at the ROHF level, using the same basis set adopted for the bulk and the reconstructed surface. The ROHF energy was found to differ from the UHF estimate by less than 0.3 kcal(mol cell)$^{-1}$.

2.5 Bond and atomic properties

The QTAM was used for characterizing the Si atomic properties and the Si–Si bond properties within and among the various layers. A thorough summary of QTAM may be found in Ref. [25]; here we recall a few key points as an introduction to the notation and quantities used in Sect. 3 and place special emphasis on those aspects that are peculiar to the study of surface systems and/or to their reconstruction processes.

QTAM is based on a generalization of Schwinger's principle [39] of stationary action so that a single principle provides the quantum mechanical description of both the total system and of its constituent atoms [25]. This generalization is unique as it applies only to those subsystems, Ω, that satisfy the variational constraint (Eq. 1) of being bounded by a surface, S, of local zero flux in the gradient vector of the electron density, $\rho(\mathbf{r})$

$$\nabla\rho(\mathbf{r}) \cdot \mathbf{n}(\mathbf{r}) = 0 \quad \forall\ \mathbf{r} \in S \tag{1}$$

The subsystems Ω are termed proper open systems [40], are defined in real space, and have the property of being the only subsystems for which observables are described by the correct Heisenberg equation of motion. Since the electron distribution for a many-electron system generally exhibits local maxima only at the nuclei [25], the quantum boundary condition given in Eq. (1) yields a

partitioning of a chemical system in a disjointed set of mononuclear regions also termed atoms in a molecule or in a crystal. As a result of this partitioning, the system average of an observable is given by a sum of atomic contributions. The number of electrons, $N(\Omega)$, the atomic net charge, $q(\Omega) = Z(\Omega) - N(\Omega)$, the first moment, $\boldsymbol{\mu}(\Omega)$, the electronic energy, $E_e(\Omega)$, and the atomic volume, $V(\Omega)$, were among the most important atomic properties evaluated for the unique basins of our slab model for the Si (111)(2 × 1) surface.

The different hybridization, or whatever departure from perfect tetrahedral symmetry of Si atoms following cleavage and surface reconstruction, may be revealed [27] by the analysis of both the individual components and the nonvanishing magnitude of the first moment of atomic distribution, $\boldsymbol{\mu}(\Omega)$. It is given as the atomic average of the electronic position vector, $\mathbf{r}_\Omega$ with the origin at the nucleus of the atom Ω, $\boldsymbol{\mu}(\Omega) = -\int_\Omega \mathbf{r}_\Omega \rho(\mathbf{r}) d\tau$, and measures the displacement of the centroid of the negative charge from the nucleus.

The electronic energy of each atom in a slab may be obtained [25] from the negative of the atomic kinetic energy, $-G(\Omega)$, since, as are all theorems derived from Heisenberg's equation of motion, the virial theorem also holds for any proper open system. When there are no forces acting on any of the nuclei in the system, the sum of electronic energies, E_e, equals the total energy, E, including nuclear repulsion. Our slab system is not at an equilibrium geometry and, therefore, one should also include in the sum the virial of the net forces acting on the nuclei to get the total energy, $E = E_e + \Sigma_\alpha \mathbf{X}_\alpha \mathbf{F}_\alpha$. In practice, since the Hellmann–Feynman forces on the nuclei, $\mathbf{F}_\alpha$, are not available within CRYSTAL98 and since approximate wavefunctions do not, in general, exactly satisfy the virial theorem – even in the case of an equilibrium geometry – the values of $-G(\Omega)$ were scaled so as to satisfy the restricted statement of the virial theorem, $T = -E$, and to thus obtain a set of atomic energies which sum to the total energy. Therefore, the changes, compared to the value in the bulk silicon, of the atomic energies of the Si atoms in the reconstructed surface include, besides changes in the usual potential-energy terms (e-n attractive energy, e-e and n-n repulsive potential energies), additional contributions arising from the virials of the net repulsive or attractive forces acting on the nuclei [25, 41].

In the case of a slab, the basins given by Eq. (1) may exhibit either an infinite volume (and their corresponding atoms may be classified as surface atoms) or a finite volume. A comparison of the atomic sizes of both cases may therefore be accomplished by selecting a particular envelope of the electron density and by defining the atomic volume as the region of space enclosed by the intersection of the atomic surface of zero flux with the chosen envelope. We used the volumes $V1$ and $V2$, which are determined using the 0.001 and 0.002 au density envelopes. A physical meaning is associated with this particular choice since $V1$ data are known [42] to give molecular sizes that are in agreement with those determined from the analysis of kinetic theory data for gas phase molecules, whereas $V2$ yields [43] molecular sizes that can be employed in describing the closer packing found in the solid state. The $V1$ volumes were found to contain more than 99.8% of the total atomic charge in any of the unique Si atoms in the slab and *a fortiori* in silicon bulk (where $V1$ equals the total volume of the silicon atom), while $V2$ may significantly differ from $V1$ for atoms in the outermost layers. We introduced [24] the dimensionless diffuseness parameter, $D = [(V1 - V2)/V1] \times 100$, as a quantitative and further index of surface character of a silicon atom in a slab.

The gradient vector field of $\rho(\mathbf{r})$ not only determines the boundary condition for a proper open system but also provides a definition of the molecular structure or, generally, of the pairwise interactions present in an assembly of atoms [25]. Two atoms Ω and Ω' are linked to one another if their nuclei are connected by a line – bond path – where $\rho(\mathbf{r})$ is a maximum with respect to any lateral displacement from the line. It has recently been shown [44] how a bond path is a universal indicator of a bonded interaction in a system in stable electrostatic equilibrium. Although the latter condition is not strictly satisfied by our slab model, we believe that the Si atoms in the adopted reconstructed surface are not so seriously displaced from their equilibrium positions so as to affect the bond path network or to significantly change the associated bond properties[1]. The point $\mathbf{r}_b$, where the density attains its minimum value along the bond path, is a critical point in $\rho(\mathbf{r})$ – that is $\nabla\rho(\mathbf{r}_b) = 0$ – and it is called a bond critical point (BCP). It has been demonstrated [45] that the local properties of $\rho(\mathbf{r})$ at the BCP sum up very concisely the nature of the interaction occurring between the two linked atoms. While the bond network in the reconstructed surface is largely anticipated on the basis of geometrical considerations only, QTAM may, in this case, be particularly useful to put on a quantitative basis the changes occurring in the Si–Si bond properties with respect to the bulk silicon and especially to the nonreconstructed surface. Among the bond properties investigated here are the displacement, Δ_{BCP}, of the BCP from the bond midpoint and the value of $\rho(\mathbf{r})$ and of its three curvatures, λ_i ($\lambda_1 \le \lambda_2 \le \lambda_3$), at the BCP. The latter are the three eigenvalues of the Hessian matrix of ρ, whose trace, given by their sum, yields $\nabla^2\rho$, the Laplacian of the electron density. The BCP is expected to be displaced towards the less electronegative Si atom, while the electron density and the parallel curvature λ_3 at the BCP are predicted [24] to increase and decrease with decreasing bond length, respectively.

We also analyzed the bond ellipticity, ε, and the ellipticity profiles along the Si–Si bond paths. ε is defined in terms of the two negative curvatures at the BCP, $\varepsilon = (\lambda_1/\lambda_2) - 1$. Analogously, one may calculate a local ellipticity value at each point of the bond path [27, 46]. The bond ellipticity is zero for Si–Si bonding in bulk and is greater than zero for any departure of the Si atomic distribution from perfect tetrahedral simmetry [24, 27]. For homopolar bonds, the ellipticity remains essentially constant over the valence regions of both bonded atoms and the value of ε at the BCP is a useful measure of the preferred spatial arrangement of the valence density [46], However, upon surface reconstruction and buckling, the Si atoms undergo different rehybridizations which may yield a significant charge transfer between bonded atoms and an appreciable displacement of their BCP from the bond midpoint. In such a case, the bond ellipticity value alone is not really indicative, while an analysis of the whole valence ellipticity profile may shed light on the preferred spatial arrangement of the valence density and on the different contributions to such a charge rearrangement arising from the two linked atoms.

The Laplacian field not only yields information on the nature of atomic interactions [25, 45] but also allows recovery [47] of the model of localized bonded and nonbonded electron pairs anticipated on the basis of the Lewis model [48]. This mapping has recently been established [49] on a firmer theoretical basis. Indeed, the local charge concentrations (CCs) displayed by the Laplacian of the electron density, the local maxima in $L(\mathbf{r}) = -\nabla^2\rho(\mathbf{r})$, signify the presence of regions of partial pair condensation, i.e., regions with greater than average probabilities of occupation by a single pair of electrons [49]. The Si1 and Si2 atoms in the Si(111)(2 × 1) surface have a nominal dangling bond, whose corresponding single localized electron should also be mapped [50, 51] or not mapped in a CC of the Laplacian field depending on the extent of bond reconstruction.

Application of QTAM to our slab model was made possible by the code TOPOND98 [52], which is interfaced [53] to CRYSTAL98 [29]. Elapsed processing times for evaluating the atomic properties of one unique Si atom in the reconstructed surface were typically as long as 40 h. The accuracy of the numerical determination of integrated properties was judged against the computed values for the atomic Lagrangian $L(\Omega) = -1/4\int_\Omega \nabla^2\rho$, a quantity that should vanish because of the atomic basin boundary condition (Eq. 1). The values of $L(\Omega)$ obtained were typically less than 2×10^{-3} au and the total number of integrated electrons differed from the theoretical value by less than 0.01e.

2.6 Scanning tunneling microscopy topography

Electron density maps, obtained from the density matrix projected onto a narrow energy region around the Fermi level, may be related

[1] When there are residual net forces on the nuclei, a bond path should be rather termed as an atomic interaction line; however, for the sake of simplicity, the bond path terminology is retained in the following.

[54] to the scanning tunneling microscopy (STM) charge densities, within the Tersoff–Hamann approximation [55]. TOPOND98 is also able to deal with these energy projected density matrices, which were evaluated with the PDIDE option of the CRYSTAL98 package [29].

3 Results and discussion

3.1 Energies

Computed relative energies of the reconstructed surface are reported in Table 1 for the various geometries and Hamiltonians, and for the ferromagnetic and antiferromagnetic solutions.

Table 1 shows that

1. The electronic structures involving rebonding of the Si1 and Si2 "dangling bond" electrons are about 20–30 kcal mol^{-1} more stable than those – ferromagnetic solution – where such rebonding is not allowed; the different behavior with respect to the Si(111)(1 × 1) surface, which has degenerate ferromagnetic and antiferromagnetic states, [59] agrees with the nearest, instead of the next-nearest, neighbor site locations of the surface dangling bonds, characterizing the reconstructed surface.
2. At variance with all kinds of DFT Hamiltonians tested by us, the HF method predicts an insulating reconstructed surface, as found experimentally [18, 19]; previous plane-wave geometry optimized LDA calculations [13, 15, 16] recover an insulating state, yet with a direct surface-state band gap (about 0.2–0.3 eV) which is less than half the experimental value from photoemission experiments [18, 19]. Thus, it is likely that even a small displacement from the equilibrium geometry or the adoption of a local basis set might lead to a conductive instead of an insulating state; such a problem does not occur with the HF method, which is known to largely overestimate the gap [56].
3. Use of an UHF formalism yields a substantial energy lowering (13–14 kcal mol^{-1}), while not significantly affecting the energy difference between the ferromagnetic and antiferromagnetic states. Besides, the UHF approach predicts a dispersion (about 0.7 eV) of the surface band along the Γ-J direction that is very close to experimental values (0.6–0.8 eV) [23] and about half of our RHF estimate (1.3 eV).
4. Adoption of LEE or MEI geometry yields comparable energies at all levels of theory.

A final comment on these energy and band results is mandatory. As widely acknowledged [56], it is not, in principle, correct to judge the quality of a periodic ab initio calculation on the basis of the agreement with the experimental band structure. Indeed, the HF and DFT Kohn–Sham one-electron eigenvalues can only be related very vaguely to this quantity which would require an adequate description of both the excited and the ground states to be appropriately calculated. Moreover, the Kohn–Sham pseudoeigenvalues do not even have the physical meaning that is attached to the HF ones by Koopmans' theorem [57]. However, because of the metallic description and the related occurrence of partially filled bands in our DFT calculations, or because of the substantial energy lowering and the much better estimate of the surface band dispersion provided by the HF method when the restricted spin–orbital constraint is released, we will give, in the following, more credit to the UHF rather than to the other descriptions of bonding and atomic properties upon surface reconstruction.

3.2 Atomic properties

A number of atomic properties for silicon atoms in the Si(111)(2 × 1) and Si(111)(1 × 1) slabs relative to bulk silicon are reported in Table 2.

3.2.1 Atomic charges

Upon reconstruction, electroneutrality is practically reached after the first two layers, as was found [24] for the nonreconstructed surface [Σq(Ω) values, Table 2], the top layer (Si1 + Si2) being, on average, negatively charged and the lower surface layer (Si3 + Si4) being positively charged. Also the polarity of the surface double layer [58] is the same in the two slabs. Conversely, the very important changes ensuing reconstruction concern the extent of surface-cell charge distortions [58], i.e. the charge separation in the double layer, the individual atomic charges which in the top layer are (UHF result) one order of magnitude greater than those in the nonreconstructed surface, and, finally, the large charge difference between the unique atoms in each layer. Indeed, at the UHF level, the net charge of each surface layer is about twice as big as that carried by two Si1L or Si2L atoms in the nonreconstructed surface, with the net negative charge of the topmost layer arising from highly negatively charged Si2 and slightly less positively charged Si1 atoms. Charge differences in the lower layer are only just less pronounced, the two unique atoms being nevertheless both positively charged (UHF result). Thus, as previously stated [12–14] the effect of buckling is to largely differentiate the unique atoms in the two surface layers; however, the electron charge was found to flow from the "up" (Si1) to the "down" (Si2) atom of the topmost layer rather than in the reverse direction as claimed before [12–14]. Inspection of bond angles

Table 1. Si(111)(2 × 1) slab. Relative energies [kcal(mol · half cell)$^{-1}$]. The notation $\alpha\alpha$ and $\alpha\beta$ refers to the initial spin setting for Si1 and Si2 atoms (see text). Electronic structure: insulating (*I*); conducting (*C*) (see text)

Geometry and spin	RHF or ROHF	UHF	Spin unrestricted DFT/B3LYP	Spin unrestricted DFT/PWGGA
LEE, $\alpha\alpha$	19.1 (I)	8.6 (I)	30.3 (C)	
LEE, $\alpha\beta$	0.0 (I)	−13.4 (I)	0.0 (C)	0.0 (C)
MEI, $\alpha\beta$	0.6 (I)	−14.7 (I)	3.1 (C)	7.4 (C)

Table 2. Atomic properties for silicon atoms in the Si(111)(2 × 1) and Si(111)(1 × 1) slabs and relative to bulk silicon. All quantities in atomic units; data for Si(111)(2 × 1) refer to the antiferromagnetic and to unrestricted Hartree–Fock (*HF*) or density functional theory (*DFT*) solutions; data for Si(111)(1 × 1) refer to the nonrelaxed (*NR*) model (see text) and the 3-21G(d) basis set; energies, ΔE, and volumes, $\Delta V1$, are given relative to bulk silicon ($\Delta X = X_{slab} - X_{bulk}$, $X = E, V1$), calculated at the restricted HF (*RHF*) or DFT/ Perdew–Wang generalized gradient approximation (*PWGGA*) level and corresponding optimum geometry, using 3-21G(d = 0.6) basis set; diffuseness is a dimensionless quantity, given by $D = (V1 - V2)/V1 \times 100$; the atomic dipole is zero for the tetrahedrally coordinated Si atom in bulk silicon

Model	Quantity	Si(111)(2 × 1)					Si(111)(1 × 1)		
		Si1	Si2	Si3	Si4	$\Sigma(\Omega)$	Si1L	Si2L	$\Sigma(\Omega)$
UHF//LEE	$\Delta E(\Omega)$	0.009	−0.151	0.033	0.106	−0.003			
UHF//MEI		0.008	−0.155	0.080	0.130	0.063			
PWGGA//LEE		0.043	−0.033	0.023	0.078	0.111			
ROHF//NR							−0.038	0.037	−0.001
UHF//LEE	$q(\Omega)$	0.138	−0.225	0.009	0.071	−0.007			
UHF//MEI		0.164	−0.248	0.009	0.076	0.001			
PWGGA//LEE		0.049	–0.077	–0.004	0.038	–0.002			
ROHF//NR							–0.019	0.016	–0.003
UHF//LEE	$\lvert\boldsymbol{\mu}(\Omega)\rvert$	0.50	0.17	0.21	0.11	–0.37[a]			
UHF//MEI		0.54	0.18	0.22	0.14	–0.30[a]			
PWGGA//LEE		0.49	0.17	0.16	0.11	–0.54[a]			
ROHF//NR							–0.23	0.06	–0.17
UHF//LEE	$D(\Omega)$	8.5	5.9	4.5	3.2	5.5[b]			
UHF//MEI		9.9	7.2	4.9	3.0	6.3[b]			
PWGGA//LEE		8.6	5.8	4.3	3.2	5.5[b]			
ROHF//NR							9.3	1.8	5.5
UHF//LEE	$\Delta V1(\Omega)$	28.2	35.3	4.8	0.5	17.2[c]			
UHF//MEI		31.1	41.9	10.0	2.9	21.5[c]			
PWGGA//LEE		34.7	32.2	5.8	1.3	18.5[c]			
ROHF//NR							25.1	2.5	13.8

[a] Sum over the μ_z components, where z is the axis perpendicular to the slab surfaces; a negative sign means that the charge is displaced outwards from the surface
[b] Average D value; the D value in the Si bulk is 0.7
[c] Average $\Delta V1$ value; the $V1$ value for the Si bulk is 138.4 au and equals the total volume of the basin

involving Si1 (LEED [7]: 109.3° and 116.8°; MEIS [9]: 108.9° and 117.8°) and Si2 (LEED: 116.8° and 121.6°; MEIS: 117.8° and 120.6°) suggests a nearly planar sp^2 arrangement for the latter and a partial sp^3 pyramidalization of the former atom. The electron flow direction obtained by us, using QTAM, complies with this geometrical arrangement and related hybridization pattern, and it is further confirmed by the very large stabilization energy found for Si2 as opposed to the small energy destabilization found for Si1 atom and by other charge rearrangements and bonding features. Our reasoning is also strengthened by the observation that the electron population and the absolute energy of Si atom increases by 0.738e and 0.192 au, respectively, on passing from the sp^3 hybridized Si in disilane to the sp^2 hybridized Si in disilene [RHF/6-311 + + G(2d,2p) calculations] [60].

Instead, the reverse electron flow direction was, in the past, initially explained by assuming that buckling of the surface chain (a Jahn–Teller type symmetry breaking) resulted in a transfer of electronic charge from the p_z dangling bond orbital of the lower atom into an energetically lower s-type dangling bond orbital on the raised atom (see discussion in Ref. 14). Later on, Badziag and Verwoerd [12], in a localized orbital analysis of their MINDO/3 cluster study of the Si(111)(2 × 1) reconstruction, proposed a mechanism which is equivalent to this but with the rehybridization of the back bonds, rather than of the dangling bonds, playing the dominant role. These authors found a net charge of −0.27e on the "up" and of 0.18e on the "down" Si atom, the electron population increase of the "up" atom being the result of a small increase (0.07e) of its p and of a larger augmentation (0.20e) of its s population, compared to the bulk. The decrease in population of the "down" atom was, on the other hand, due to a noteworthy lowering (0.31e) of its p population, only partly compensated for by a moderate increase (0.13e) in its s population. In practice, despite the fact that the occupied dangling bond orbital on Si1 in their model is almost completely p_z in character, Badziag and Verwoerd [12] found a very little net increase in the total p electronic charge on this atom. Conversely, they found a high (45–50%) s content on all of the σ bonds in which chain atoms participate as a result of an overall transfer of p charge from the "down" atom to the s charge associated with the back bonds of the raised atom. More recent SLAB–MINDO calculations [14] confirmed the net electron flow from the Si2 to Si1 atom, yet this was accompanied by a slight decrease in the s charge on each raised atom and a significant increase in its total p charge, nearly all of which goes into its occupied dangling bond. Both MINDO analyses [12, 14] agreed in refusing π bonding as the major driving force behind the chain model, a conclusion partially consistent with our study, despite the opposite direction found by us for the electron flow in

the topmost layer. Still, how can this reverse flow be explained? Is this the result of the adopted computational model or rather of the different partitioning scheme used to define the atomic populations? Mulliken's analysis of the spin-polarized wavefunctions assigns small negative charges to Si2 (−0.053e and −0.003e at the UHF//LEE and PWGGA//LEE level) and either negligible positive (0.002e, UHF//LEE) or small negative charges (−0.034e, PWGGA//LEE) to Si1. Conversely, Si1 is predicted to be negatively charged (−0.134e) and Si2 to be positively charged (0.093e) by Mulliken's analysis at the RHF//LEE level. Thus, using a partitioning of electrons in the space of the basis functions, we recover either (non spin-polarized solution) the same charge transfer direction as found previously [12–14] or very small charge fluxes whose directions depend on the kind of spin-polarized Hamiltonian adopted. Instead, using QTAM partitioning, the Si2 atom was always found to be negatively charged and the Si1 atom was always found to be positively charged, with the non-spin-polarized solution (RHF//LEE) yielding a large further strengthening of the electron flow from Si1 ($q = 0.520$) to Si2 ($q = -0.550$).

It is also interesting to investigate how the electronic perturbation caused by cleaving and ensuing surface reconstruction propagates and dampens through the first Si atoms layers[2]. In the hydrogen-covered and clean Si(111)(1 × 1) slabs, Si atoms were found to exhibit bulk populations beginning from the fourth layer inwards [24]. The surface reconstruction occurring in Si(111)(2 × 1) induces appreciable charge distortions up to and including the fourth layer (Si5 + Si6 = −0.023e; Si7 + Si8 = 0.048e; UHF//LEE), while from the fifth layer inwards the layers and their unique atoms may be considered as practically neutral within integration error. The large net charge found for the fourth layer agrees with its significant subsurface relaxation [7].

While there is a limited effect of geometry on the net charges in the first layers (compare UHF//LEE and UHF//MEI results), larger differences arise by using the spin-polarized DFT instead of the UHF approach. DFT predicts the same double layer polarity as the UHF model, but with much less charge separation between the layers. Net atomic charges at the PWGGA//LEE level are about one-third of the UHF ones for the topmost layer. Such differences are probably to be ascribed to the metallic, rather than insulating, description obtained for the reconstructed surface at the DFT level.

3.2.2 Atomic first moments

The magnitudes, $|\boldsymbol{\mu}(\Omega)|$, of the atomic first moment of the Si atoms in the surface layers are listed in Table 2, while Fig. 2 shows the nonvanishing components, normal (z) and parallel (y) to the surface for the UHF//LEE case. The Si atoms undergo a drastic change in their polarizations, from the only z direction exhibited in the nonreconstructed surface to comparable and very large polarizations, normal and parallel to the slab surface in the reconstructed system. Figure 2 is a pictorial, yet quantitative, representation of one of the important effects ensuing the formation of a new 2D compound [1] upon surface reconstruction. The polarization magnitudes of Si1 or Si2 atoms are, respectively, twice as big or just a little smaller than those of Si1L in the Si(111)(1 × 1) surface. The atomic first moment magnitudes of Si3 and Si4 are 2–3 times larger than those of Si2L atoms in the nonreconstructed surface.

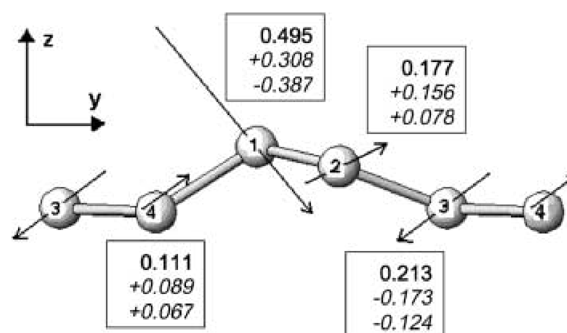

Fig. 2. Atomic first moments, $\boldsymbol{\mu}(\Omega)$, of the atoms in the topmost and lower surface layers of the Si(111)(2 × 1) surface. The *arrows* [unrestricted Hartree–Fock (*UHF*)//LEE results] are directed as $\boldsymbol{\mu}(\Omega)$ (from the negative to the positive centroid of atomic charge) and their length is proportional to $|\boldsymbol{\mu}(\Omega)|$. The values in atomic units of $|\boldsymbol{\mu}(\Omega)|$, μ_y and μ_z are reported in a *box*, from top to bottom, for each atom

The "up" atom (Si1) is significantly polarized outwards ($\mu_z = -0.39$ au; UHF//LEE), even more than the Si1L atom ($\mu_z \equiv \boldsymbol{\mu} = -0.23$ au) in the Si(111)(1 × 1) surface, which has a localized unpaired electron in an sp^3 dangling bond [24] Conversely, the "down" atom (Si2) exhibits a much smaller ($\mu_z = 0.08$), and directed inward, component of the polarization normal to the surface. The dominant polarization component of Si2 atom is directed parallel to the surface ($\mu_y = 0.16$) and places electronic charge along the Si2–Si1 bond, while this same component in Si1 ($\mu_y = 0.31$) is directed so as to remove charge from the bond. These different polarizations of the up and down atoms agree with a big electron population in a dangling sp^3 orbital (pointing towards $+z$) of the Si1 atom and with preferential electronic charge accumulations towards the Si1 atom in Si2.

The outward polarization of surface atoms is typical [58] of a finite monoatomic crystal and, as mentioned earlier, was recovered in the nonreconstructed surface [24]. The 2D reconstruction occurring in Si(111)(2 × 1) also yields a net outward polarization for the topmost layer, as a result of the prevailing outward polarization of Si1 over the inward polarization of Si2 atoms. The Si1 centroid (computed from $-\mu_{z,\Omega}/N_\Omega$) is displaced 0.028 au outwards, while that of Si2 is displaced only 0.005 au inwards (Si3 = 0.008 au outwards, Si4 = 0.005 au inwards). The corresponding displacements in the unrelaxed surface are 0.016 au outwards (Si1L) and 0.004 au (Si2L) inwards.

Finally, we note that the qualitative picture of atomic polarization was found to be independent of the geometry and the method used to compute the electronic structure of the reconstructed surface.

[2] For the sake of conciseness these results are not reported in the table but can be obtained upon request

3.2.3 Atomic energies

Atomic energies are given in Table 2 relative to bulk silicon [$\Delta E(\Omega) = E(\Omega)_{slab} - E(\Omega)_{bulk}$] for the atoms of the first two layers. Before discussing the reported energy changes, it is worth recalling (see Sect. 2) the exact meaning of such quantities in our nonequilibrium slabs and to also point out the following:

1. The average destabilization, ΔE_{av}, of the unique atoms in the Si(111)(2 × 1) slab at the UHF//LEE level is 0.011 au; this means that a $\Delta E(\Omega)$ value of 0.011 au represents the average change in the energy content of a Si atom in our reconstructed slab compared to the bulk (the ΔE_{av} value for UHF//MEI and PWGGA//LEE is 0.009 au).
2. As shown in previous work on the hydrogen-covered and clean Si(111)(1 × 1) surfaces [24], atomic energies are not expected to converge towards the bulk Si value even for the atoms of the innermost layers, although their populations and bond properties show almost perfect convergence. For instance, in the Si(111)(1 × 1) slab, the Si4L and Si5L atoms have a ΔE value of 0.060 au in spite of their bulklike nature for all the other properties investigated [24]. Indeed surfaces have an important effect on the binding energies of electrons, through the creation of a double layer and its associated electric field on each face of the crystal [58]. Distortions in the electronic charge distributions near the surface affect the energies of electronic levels well inside, owing to the long range of the Coulomb potential, and, as a consequence, also affect the total energy of atoms. Thus, the energy values for the atoms in the slab, in contrast to the case of those for an ideal infinite crystal (as is our computed bulk silicon), are consistent with the correct work function for the electrons in the crystal [56].
3. The energies of atoms of the surface layer (Si1–Si4) should not be affected, to first order, by the surface electric field because this field is just the result of their perturbed charge distribution.

Keeping in mind all these "caveats", it is possible to observe and conclude the following:

1. Analogously to the nonreconstructed surface, the top layer (Si1 + Si2) atoms are (UHF results), on average, energy-stabilized, while those (Si3 + Si4) of the lower surface layer are both destabilized compared to the bulk silicon. However, in agreement with the increased charge transfer upon reconstruction, the average energy changes are about twice as large [$(\text{Si1} + \text{Si2})_{av} = 0.071$ au; $(\text{Si3} + \text{Si4})_{av} = 0.069$ au] as those in the unrelaxed Si(111)(1 × 1) slab (Si1L = −0.038 and Si2L = 0.037 au).
2. Although notably charge-depleted the "up" atom of the topmost layer has an energy close to the bulk value, probably the result of the increased s character of its back bonds; the "down" atom is highly stabilized (−0.151 au, UHF//LEE) as anticipated by its large negative charge.
3. There is (UHF calculations) a marked influence of geometry on the energy stabilization of the surface double layer. While the LEE model predicts an average atomic energy content quite close to that of the bulk and of the double layer in the nonreconstructed surface, the MEI geometry describes the first two layers as overall destabilized (compare $\Sigma\Delta E_{\Omega}$ values in Table 2). As for this discrepancy in the double layer energy estimation, we are inclined to give more credit to the LEE results because of the more accurate description of buckling in the first layers afforded by the LEED structural determination.
4. The metallic description provided by DFT for the reconstructed surface leads to a net energy destabilization for both the top and lower layers of surface atoms.
5. At variance with Si(111)(1 × 1), where the $\Delta E(\Omega)$ values reach a steady value beginning from the third layer inwards, the atomic energies of the reconstructed surface change from layer to layer and differ for the two unique atoms of each layer because of buckling. This behavior agrees with the deep propagation into the lattice of the topological changes occurring in the surface layer upon reconstruction [7]. The atomic energies are found to dampen their oscillations only beginning from the sixth layer inwards.

3.2.4 Atomic volumes

The $V1$ value for the Si bulk amounts to 138.4 au and equals the total volume of the basin. The diffuseness, D, of the Si atom in the bulk is very close to zero ($D = 0.6$), since its $V2$ value nearly coincides ($V2 = 138.6$ au) with $V1$. The D values and the changes in volume $\Delta V1 = V1_{slab} - V1_{bulk}$ for the surface atoms in the reconstructed and in the unrelaxed Si(111) surface are listed in Table 2. The $\nabla\rho$ trajectories originating from nuclei, and the intersections of the zero-flux surfaces defining Si atomic basins, in the two mirror planes normal to the surface of the reconstructed slab are displayed in Fig. 3. One of these planes contains Si1 and Si4 nuclei and the other contains Si2 and Si3 nuclei. As suggested by Fig. 3, only the atoms of the topmost layer have their volumes largely increased compared to the bulk, while the atoms of the lower surface layer, in particular Si4, are very much less perturbed. This observation agrees with the $\Delta V1$ values reported in Table 2, which shows (UHF//LEE data) a 20–25% volume expansion for Si1 and Si2, a 3% inflation for Si3, and only a negligible volume increase for Si4. The values of D for the four unique atoms of the surface layer point out the large deviation of their electronic distribution from the bulk. On average, more than 5% of the volume of their $V1$ atomic basins, instead of the only 0.6% in the bulk, is characterized by an electron density lower than 0.002 au and even their lowest D value, occurring for the Si4 atom, is 5 times bigger than in the bulk. These large D values denote the nonnegligible surface character of the atoms in the lower surface layer despite the small $\Delta V1$ values found for the Si3 and especially the Si4 atoms. Silicon atoms from the third layer inwards

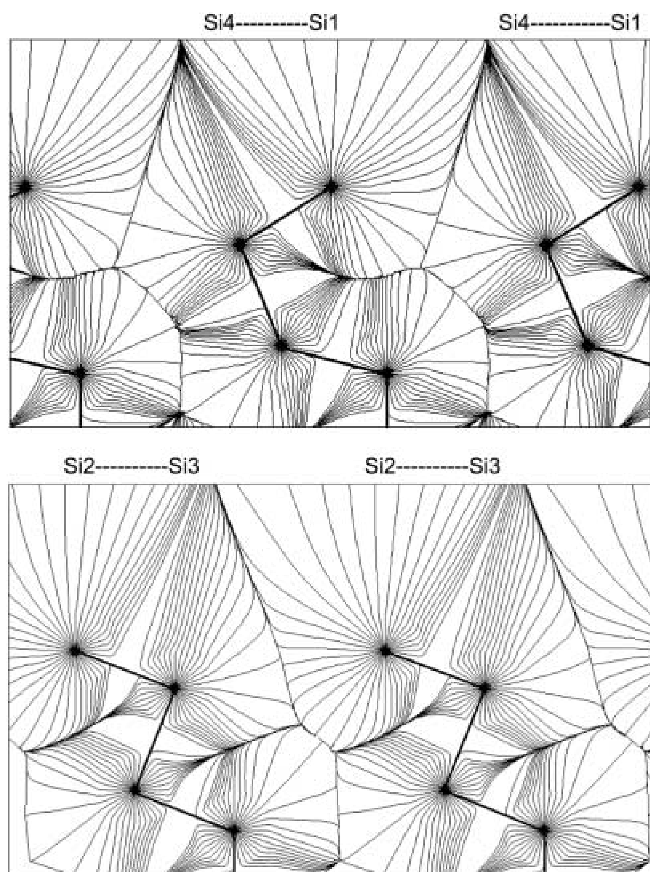

Fig. 3. Downhill $\nabla\rho$ trajectories (originating from the nuclei) in the two mirror planes normal to the Si(111)(2 × 1) surface and containing (*top panel*) Si1 and Si4 and (*bottom panel*) Si2 and Si3 nuclei. The collection of these $\nabla\rho$ trajectories defines the atomic boundaries in the two mirror planes; Si1 and Si2 have their atomic volume largely increased compared to the bulk silicon, while the atoms of the lower surface layer are much less expanded (UHF// LEE results)

exhibit D values very close to that of the bulk, although the large oscillations (127–142 au) in the $V1$ values found for the atoms up to and including the fifth layer confirm that these atoms experience significant subsurface relaxations.

The larger $V1$ volume found for Si2 compared to Si1 does not indicate a greater "surface" character of the former atom, rather it reflects its larger electron population since the two atoms exhibit a similar electronic charge dilution ($V1/N = 12.1$ au) compared to the bulk ($V1/N = 9.9$ au). Moreover, Si1 has a diffuseness which is about 40% larger than in the Si2 atom, probably a result of the diffuse distribution of its partially unpaired electron.

Comparison with data for the Si(111)(1 × 1) surface shows that upon reconstruction the atoms of the topmost layer are, on average, less diffuse than the Si1L atoms in the unrelaxed surface [D_{av}(Si1,Si2) = 7.2; D(Si1L) = 9.3], the opposite being true for the atoms of the lower surface layer [D_{av}(Si3,Si4) = 3.8; D(Si2L) = 2.5]. Thus, reconstruction affords a greater equalization of the "surface" characteristics of the atoms in the first two layers, the average value of D in the recontructed surface for these layers ($D = 5.5$, UHF// LEE) being exactly equal to that of the unrelaxed surface (Table 2).

The $V1$ and D values of the Si1 (reconstructed surface) and the S1L atoms (unrelaxed surface) are very much alike, thus once more confirming the presence of a (partially) unpaired electron in the former atom.

3.3 Bonding properties

In the top panels of Fig. 4, contour plots of $\rho(\mathbf{r})$ and $L(\mathbf{r})$, in planes containing the unique bond paths among the atoms of the two outermost layers, are placed side by side so as to show the whole surface bonding network in the Si(111)(2 × 1) system. Figure 4 clearly reveals that surface reconstruction leads to important differences among the electron density distributions along each of these bonds. The properties of the bonds among the atoms of the second (Si3,Si4) and third layer are, on the other hand, much less differentiated and already closer to those of the bulk, especially for the value of the electron density, ρ_b, at the bond critical point (BCP). Thus, the portrait of the ρ and $\nabla^2\rho$ distributions along these latter bonds may be used as a qualitative reference to visually appreciate the differences among the surface bond charge distributions and their own departures from that of the bulk. The perturbations induced by surface reconstruction are then made quantitative in Table 3, where the bond properties in the first two layers of the Si(111) reconstructed and nonreconstructed surfaces are compared with those of the bulk. The first very important observation is that in the reconstructed surface the average ρ_b value for these surface bonds is either equal to (UHF//LEE, $\rho_{b,av} = 8.49$ au) or even slightly larger than (PWGGA//LEE, $\rho_{b,av} = 7.66$ au) the ρ_b value in bulk silicon ($\rho_b = 8.49$ and 7.63 au for RHF and DFT/PWGGA, respectively). Such behavior is not observed for the MEI geometry [9], which is, however, less reliable as far as the geometrical distortions in the first layers are concerned (see earlier). It is worth noting that in the unrelaxed surface and at variance with what was found (UHF//LEE) following reconstruction, the Si1L–Si2L bonds are slightly weakened compared to the bulk (ρ_b decreases by about 1% and the parallel curvature, λ_3, increases by about 3%). This interesting result must be taken with some caution since our systems are not at their equilibrium geometry. Yet, we have previously shown [24] how a geometrical and basis set optimization (TR model in Ref. [24]) leads to a notable further weakening of the Si1L–Si2L bond in the unreconstructed surface.

Inspection of the individual properties of the surface bonds reveals that the Si1–Si2 bond is significantly shortened and strengthened compared to the bulk, while the other bonds are either appreciably weakened (Si3–Si4 and Si1–Si4) or hardly strengthened (Si2–Si3) upon reconstruction. These qualitative considerations hold true for all the methods and geometries investigated, with the only exception of the Si2–Si3 bond, which is predicted to be weakened, rather than hardly strengthened, by the UHF//MEI model. As expected

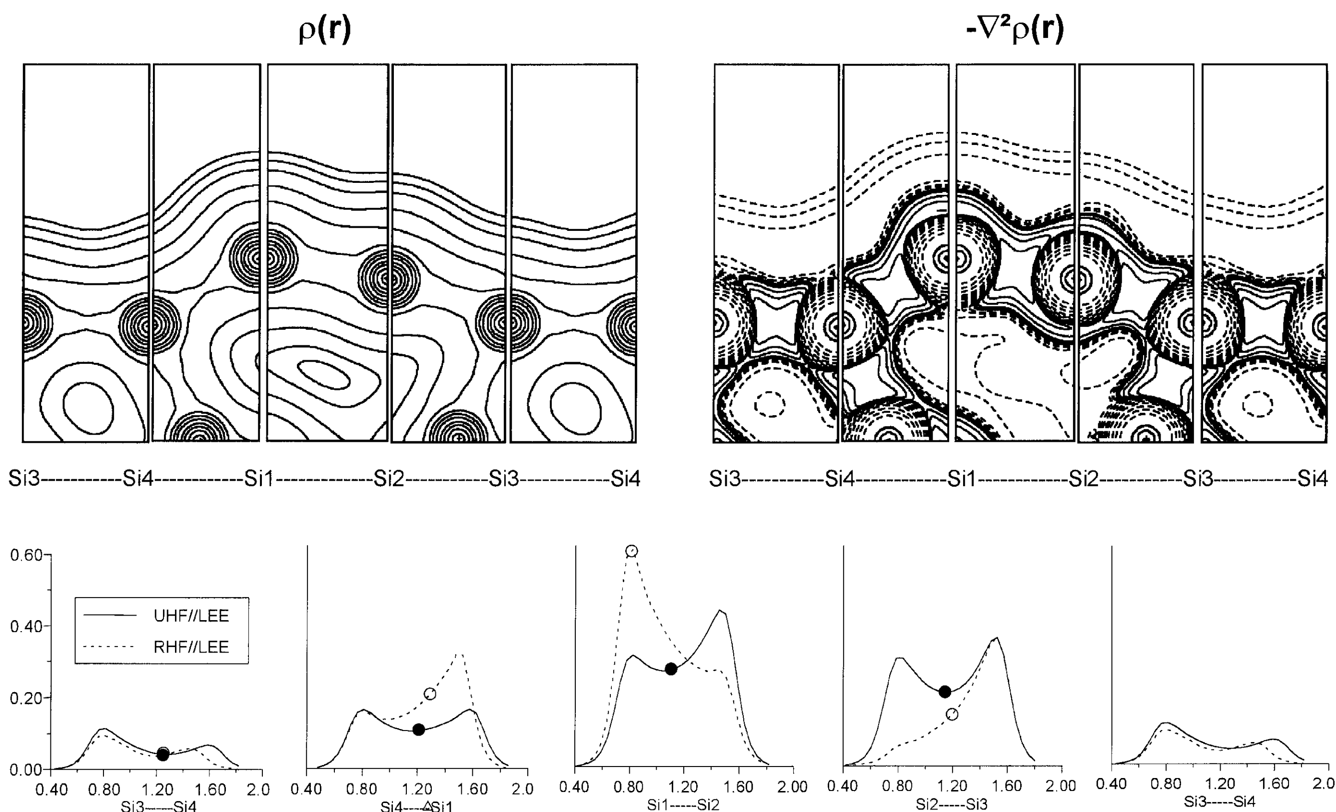

Fig. 4. *Top*: contour plots of $\rho(\mathbf{r})$ (*left panel*) and $L(\mathbf{r}) = -\nabla^2\rho$ (*right panel*) in planes normal to the Si(111)(2 × 1) surface and containing the unique bond paths among the atoms of the two outermost layers. Contour plots in five different planes are placed side by side so as to show the whole surface bonding network. Results from UHF//LEE model. *Bottom*: ellipticity profiles (see text) along the bond path of each pair of bonded atoms in the two outermost layers of the Si(111)(2 × 1) surface. The position, along each bond path, of the bond critical point is indicated by a *dot*. Results from UHF//LEE and restricted Hartree–Fock (*RHF*)// LEE models

from its supposed partial π character and as mentioned earlier, the largest change with respect to the Si–Si bond in the bulk is found for the Si1–Si2 bond which, at the UHF//LEE level, has its ρ_b and $-\nabla^2\rho_b$ values increased by about 6 and 9% and λ_3 decreased by approximately 36%. The electron distribution along Si1–Si2 is not symmetric with respect to the bond midpoint (Fig. 4) and the BCP is, as a consequence, significantly displaced (0.054 Å, UHF//LEE) towards the less electronegative Si1 atom (see earlier). Such a displacement, which is the biggest among those found for the surface bonds (compare $|\Delta_{BCP}|$ values in Table 3), reflects the different nature of the Si1 and Si2 atoms and is one of the signs of the departure of the real charge distribution from what one would surmise for the π-conjugated topmost chain in the nonbuckled geometry of the PC model. As clearly evident from Table 3, all the surface bonds in the reconstructed surface have significant ellipticity, with only Si3–Si4 showing a value close to zero ($\varepsilon = 0.02$–0.03) and quite similar to that ($\varepsilon = 0.04$) of Si1L–Si2L in the unrelaxed surface. As expected, the major axis [25] of the charge distribution is always directed normal to the surface and the largest ε value is found along the supposedly π-bonded chain ($\varepsilon = 0.26$–0.30). The notable ellipticity of the neighboring bonds (Si2–Si3 and Si1–Si4) reveals that the π conjugation is not strictly localized along the topmost layer chains, but it extends over a 2D array of bonds between the topmost and the lower surface layers. The asymmetry of bonding interactions in these layers is then made manifest by the ellipticity profiles along the bond paths (Fig. 4, bottom panels). These profiles (UHF//LEE data) confirm the Si1–Si2 bond as the most asymmetric, with the charge distribution in the Si2 basin showing the largest deviation from cylindrical symmetry and the greater accumulation of charge in the π direction. We found that the asymmetry of the bond ellipticity profiles in the reconstructed surface is strongly influenced by the release of the double occupancy constraint, while it is hardly affected by change of geometry (LEE, MEI) or of general computational model (HF, DFT). Comparison at the RHF//LEE and UHF//LEE levels of the ellipticity profiles along the Si1–Si2 and Si2–Si3 bonds shows (Fig. 4) that the spin-polarized solution allows a smaller differentiation within each pair of bonded atoms and a more efficient π delocalization of the surface bonds. Such a change is accompanied by a significant energy stabilization of the reconstructed surface (see earlier). It is also worth noting that UHF and RHF differ in the qualitative description of the charge accumulation along the π chain, since in the non-spin-polarized solution the largest ellipticity values are found in the basin of the "up" rather than in that of the "down" atom.

Table 3. Bond properties of Si(111)(2 × 1) and Si(111)(1 × 1) slabs as compared to bulk silicon. If not otherwise stated, all quantities are in atomic units; reported data are from the same methods, geometries and magnetic solutions as in Table 2; Δ_{BCP} is the distance from the bond critical point (*BCP*) to the midpoint of bond X-Y: a positive value for Δ_{BCP} indicates that the BCP is closer to the X atom; for the meaning of the other symbols, see text

Model	Bond, X-Y	R (Å)[a]	Δ_{BCP} (Å)	$\rho_b \times 100$[a]	$-\nabla^2\rho_b \times 100$[a]	$\lambda_3 \times 100$[a]	ε
Si(111)(2 × 1)							
UHF//LEE	Si1—Si2	2.273 (−4.1)	0.054	8.99 (5.9)	12.5 (8.5)	1.7 (−36.2)	0.26
UHF//MEI		2.261 (−4.6)	0.068	9.11 (7.3)	13.1 (13.2)	1.5 (−44.9)	0.25
PWGGA//LEE		2.279 (−4.1)	0.036	8.16 (6.9)	8.3 (6.1)	3.8 (−7.7)	0.29
UHF//LEE	Si1–Si4	2.383 (0.5)	−0.014	8.10 (−4.6)	10.3 (−10.7)	2.8 (5.3)	0.08
UHF//MEI		2.446 (3.2)	−0.042	7.56 (−11.0)	8.9 (−22.8)	3.0 (12.8)	0.07
PWGGA//LEE		2.389 (0.5)	0.035	7.22 (−5.4)	6.7 (−15.2)	4.2 (2.4)	0.10
UHF//LEE	Si2–Si3	2.308 (−2.7)	−0.026	8.67 (2.1)	11.9 (2.7)	2.4 (−10.2)	0.12
UHF//MEI		2.374 (0.1)	0.009	8.03 (−5.4)	10.0 (−13.5)	2.8 (3.8)	0.12
PWGGA//LEE		2.314 (−2.7)	−0.010	7.85 (2.9)	7.9 (0.8)	4.2 (1.9)	0.09
UHF//LEE	Si3–Si4	2.391 (0.8)	−0.036	8.21 (−3.3)	10.7 (−7.3)	2.8 (6.4)	0.03
UHF//MEI		2.418 (2.0)	−0.034	7.98 (−6.0)	10.0 (−13.3)	3.0 (13.2)	0.02
PWGGA//LEE		2.397 (0.8)	−0.026	7.39 (−3.1)	7.2 (−8.4)	4.3 (3.9)	0.03
Si(111)(1 × 1)							
ROHF//NR	Si1L–Si2L	2.371	−0.001	8.40 (−1.2)	11.1 (−4.1)	2.7 (3.0)	0.04
Si bulk							
RHF	Si–Si	2.371	0.000	8.49	11.6	2.6	0.00
PWGGA		2.377	0.000	7.63	7.9	4.1	0.00

[a] In *parentheses* percentage changes, $[100(X_{slab} - X_{bulk})/X_{bulk}$, $X = \rho_b, -\nabla^2\rho_b, \lambda_3]$, with respect to bulk silicon

The Si1–Si2 bond asymmetry is also revealed by the Laplacian distribution (Fig. 5). All the models investigated, and regardless of the geometry adopted for the reconstructed surface, find a single nonbonded charge concentration (NBCC) in the Si1 and none in the Si2 atomic basin[3]. The NBCC of Si1 – associated with a nominal dangling bond of Si1 directed outwards from the surface – is characterized by L and ρ values that are 50 and 38% less (UHF//LEE results) than those of a bonded charge concentration (BCC) in bulk silicon. Smaller decreases (40 and 34%, respectively) are, on the other hand, found for the NBCC of the dangling bond of the Si1L atom in the nonrelaxed surface. Thus, upon reconstruction, the single electrons associated with the nominal dangling bonds of the three-coordinated atoms either (Si2 atom) participate entirely in bond reconstruction or (Si1) are somewhat more involved in rebonding than the Si1L atoms in the Si(111)(1 × 1) surface. As shown in Fig. 5, the RHF model predicts a NBCC on the Si1 atom that is larger than that computed with the spin-polarized approach and, more importantly, that is even bigger than that found for Si1L in the nonreconstructed surface. This result shows that the RHF method is unable to properly describe the bond reconstruction in the PC model of the Si(111)(2 × 1) surface and further confirms that the spin-polarized solution allows a smaller differentiation of the Si1 and Si2 atoms and a more efficient π delocalization of the surface bonds.

[3] A very small NBCC, directed towards the interior of the slab and whose $L(\mathbf{r})$ value is less than one-third of the value of a BCC in the bulk, was actually found on the Si2 atom in the case of the UHF//LEE model

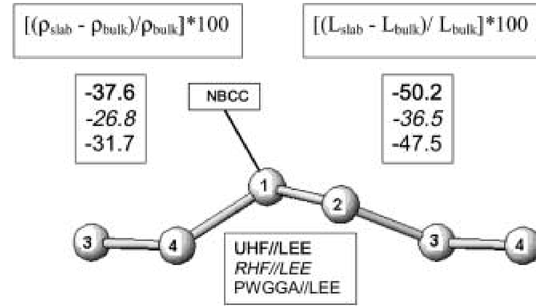

Fig. 5. Percentage changes of ρ and of $L = -\nabla^2\rho$ values at the $L(\mathbf{r})$ nonbonded charge concentration (*NBCC*) of the Si1 atom with respect to the corresponding values at a bonded charge concentration in Si bulk

The differences of the RHF and UHF descriptions of Si(111)(2 × 1) surface are also mirrored in the related band structures (Fig. 6, top). As said previously, the RHF model overestimates the surface band dispersion along the Γ-J direction, while the UHF description is much closer to experiment. It is interesting to evaluate how these differences affect the contour plots of the STH charge density [54] which may be obtained, within the Tersoff–Hamann approximation [55], from the density matrix projected onto a narrow region around the Fermi level. We used an energy window of 1.3 eV, corresponding to a bias voltage of 1.3 V between the STM probe and the surface, so as to sample the whole bandwidth of the RHF surface states. The STM charge densities in five planes normal to the surface and containing the unique nuclei of the two outermost surface layers are displayed in Fig. 6 (bottom panels). As revealed by Fig. 6, the dominant contribution to the surface states comes from the atoms of the topmost layer (Si1 and Si2) in both computational approaches.

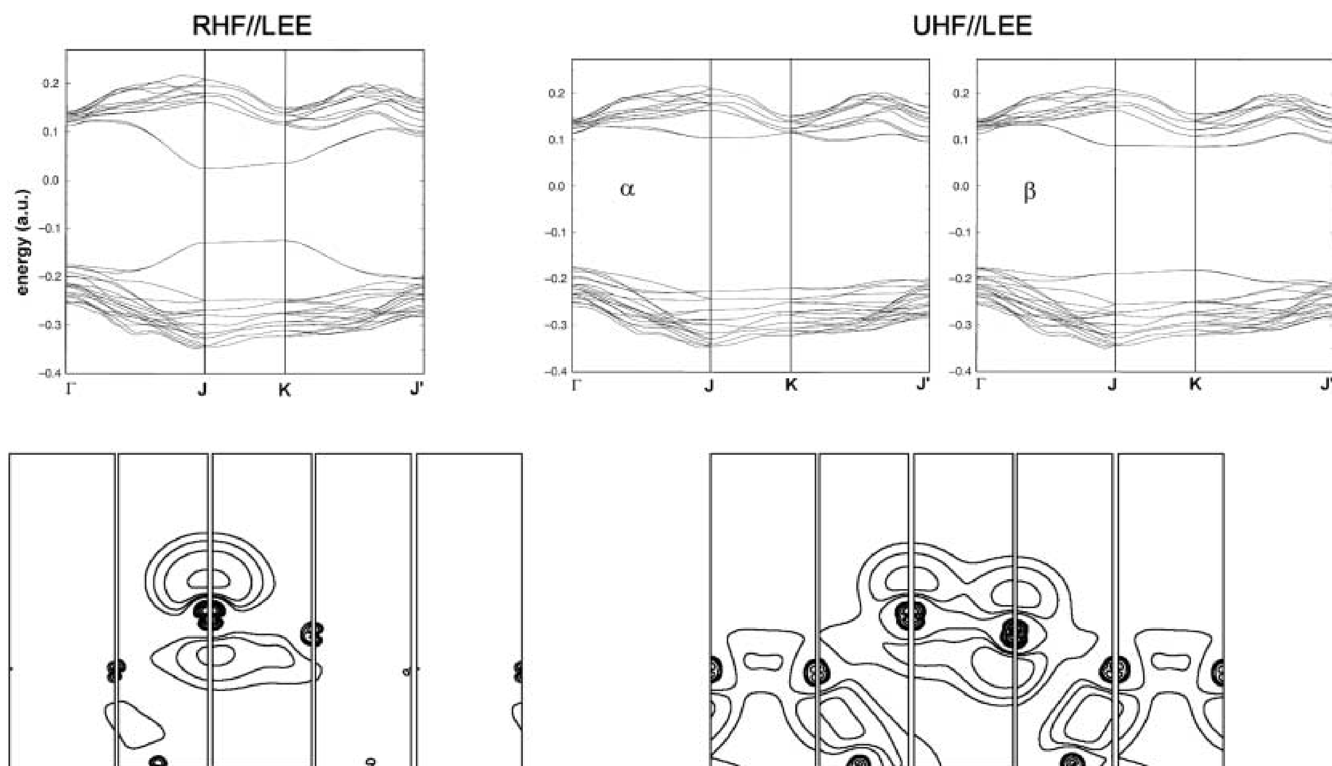

Fig. 6. *Top*: band structure for the Si(111)(2 × 1) surface at the (*left panel*) RHF//LEE and (*right panel*) UHF//LEE levels. *Bottom*: electron density maps obtained from the RHF//LEE (*left panel*) and UHF//LEE (*right panel*) density matrices projected onto a 0.05 au energy window below the Fermi level. Contour plots refer to the same five planes of Fig. 4. These maps may be related [54] to the scanning tunneling microscopy images, within the Tersoff–Hamann approximation [55]. The contour values (in atomic units) increase from the outermost one inwards in steps of 2×10^n, 4×10^n, and 8×10^n, with n beginning at −3 and increasing in steps of 1

Yet, at the tunneling voltage investigated, the RHF method predicts a very large asymmetry in the STM densities above these atoms, with only the Si1 atom exhibiting a significant density on top of it. This result agrees with the larger NBCC on the Si1 atom and with the high asymmetry in the π conjugation (see ellipticity profiles) recovered at the RHF level. Conversely, the UHF description predicts the contributions of Si1 and Si2 atoms to be very much alike.

4 Conclusions

By using a slab model for the surface, and by performing periodic first principles calculations, at geometries taken from experiment, we have investigated the bond and atomic properties of the silicon atoms in the π-bonded chain reconstructed Si(111)(2 × 1) system. The effect on these properties of the chosen slab geometries and of the kind of computational models adopted has been discussed in some detail.

Making use of the QTAM to analyze the computed wavefunctions has enabled us to provide a direct-space description and understanding of the Si(111)(2 × 1) surface reconstruction, thereby improving the still insufficient chemical knowledge on this prototype of clean semiconductor surfaces. Adoption of bulk silicon and the ideal Si(111)(1 × 1) nonrelaxed surface as suitable reference systems has allowed the changes in chemical properties ensuing surface reconstruction to be placed on a quantitative and relative basis.

As in the case of the unrelaxed surface, the Si(111)(2 × 1) system exhibits an uncharged double layer surface structure, yet with much larger surface-cell charge distortions [58]. Indeed, upon reconstruction, the charge separation in the double layer is largely increased and the atomic charge of the unique atoms in the top layer enhanced by 1 order of magnitude. The effect of buckling is to largely differentiate the atoms of each surface layer. For example, the topmost surface layer is negatively charged as in the unrelaxed surface but its net negative charge is the result of highly negatively "down" and slightly less positively charged "up" Si atoms. The direction of the charge transfer in the topmost chain is opposite to that claimed previously [12–14], but it agrees with both the bond angles and related hybridization patterns of the two atoms involved and their relative energy. The reason for such a discrepancy was found to lie mainly in the method used to partition the electrons among the atoms, although important effects due to the kind of ab initio approach adopted have also been highlighted.

One of the most clear-cut effects due to the formation of a new 2D compound, following surface reconstruction, is the drastic change that the atomic polarizations of the surface layer atoms undergo from the only, normal to the slab, direction exhibited in the nonreconstructed surface to the comparable and larger

polarizations, normal and parallel to the slab surface, found in the reconstructed system.

According to the increased charge transfer upon reconstruction, the average energy changes in the topmost and lower surface layers are about twice as large as those in the unrelaxed slab. At variance with what was found in the Si(111)(1 × 1) system, the atomic energies of the succeeding layers in the reconstructed surface change from layer to layer and differ for the two unique atoms of each layer, because of buckling. This is the result of the deep propagation into the lattice of the geometrical changes occurring in the surface layers upon reconstruction.

The properties of the Si–Si bonds in the first two layers of the Si(111)(2 × 1) surface suggest that these bonds are, on average, as strong as in the bulk, in contrast to what was found for the unrelaxed surface where the related Si1L–Si2L bonds are slightly weakened. Reconstruction affords a partial involvement in rebonding of the single electrons associated with the nominal dangling bonds of the Si1 and Si2 atoms, thus yielding the average strengthening mentioned, compared to the unrelaxed slab, of the bonds within and between the topmost and lower surface layers. As previously stated [12–14] π bonding is not completely realized along the topmost chain and does not constitute the only driving force behind the PC model. The nature, the extent, and the asymmetry of π conjugation in the topmost chain has been thoroughly investigated. The Si1–Si2 bond electron distribution, although displaying the largest deviation from the cylindrical symmetry and the greater accumulation of charge in the π direction, is highly asymmetric along the bond path, in agreement with the differences in the atomic properties of these two atoms. Significant ellipticities were also found for the neighboring bonds (Si2–Si3 and Si1–Si4), thus indicating that the π conjugation is not strictly localized along the topmost layer chains, but that it rather extends over a 2D array of bonds between the topmost and the lower surface layers.

We have also shown how the adoption of a spin-polarized, instead of a conventional nonpolarized, solution leads to a smaller differentiation within each pair of bonded atoms and to more efficient π delocalization of the surface bonds. This change of description involves a significant energy stabilization of the reconstructed surface. Differences in the spin-polarized and nonpolarized model approaches are also reflected in the computed surface band dispersion along the reciprocal lattice direction associated with the π chain in the real space and in the STM charge density portraits.

This study further confirms the ability of QTAM to shed light on the changes in bonding and atomic properties of Si in a variety of perturbed diamond-like silicon lattices. The peculiar properties of the new 2D silicon compound [1], formed through the PC 2 × 1 surface reconstruction, have been quantitatively characterized.

Further work along these lines is currently under way in our laboratory for investigating important surface effects on ultrahigh vacuum (100) cleaved Si when this system is exposed to passivation treatment with hydrogen to provide its long-term protection against oxidation and adsorption of impurities.

Acknowledgements The authors acknowledge financial support by CNR under project “Materiali Speciali per Tecnologie Avanzate II”

References

1. Duke CB (1995) Chem Rev 96: 1237
2. Neergard Waltenburg H, Yates JT (1995) Chem Rev 95: 1591
3. Srivastava GP (1997) Rep Prog Phys 60: 561
4. Lander J, Gobeli GW, Morrison J (1963) J Appl Phys 34: 2298
5. (a) Pandey KC (1981) Phys Rev Lett 47: 1913; (b) Pandey KC (1982) Phys Rev Lett 49: 223
6. (a) Northrup JE, Cohen ML (1982) Phys Rev Lett 49: 1349; (b) Northrup JE, Cohen ML, Physica B (1983) 117/118: 761
7. Himpsel FJ, Marcus PM, Tromp R, Batra IP, Cook MR, Jona F, Liu H (1984) Phys Rev B30: 2257
8. Feder R, Monch W (1984) Solid State Commun (1984) 50: 311
9. Smit L, Tromp RM, Van Der Veen JF (1985) Surf Sci 163: 315
10. Sakama H, Kawazu A, Ueda K (1986) Phys Rev B 34: 1367
11. Bechstedt F, Reichardt D (1988) Surf Sci 202: 58
12. Badziag P, Verwoerd WS (1988) Surf Sci 201: 87
13. Ancilotto F, Andreoni W, Selloni A, Car R, Parrinello M (1990) Phys Rev Lett 65: 3148
14. Craig BI, Smith PV (1990) Surf Sci 225: 225
15. Northrup JE, Hybertsen MS, Louie SG (1991) Phys Rev Lett 66: 500
16. Lee S-H, Kang M-H (1996) Phys Rev B 54: 1482
17. (a) Chiaradia P, Cricenti A, Selci S, Chiarotti G (1984) Phys Rev Lett 52: 1145; (b) Olmstead MA, Amer NM (1984) Phys Rev Lett 52: 1148; (c) Ciccacci F, Selci S, Chiarotti G, Chiaradia P (1986) Phys Rev Lett 56: 2411
18. Uhrberg RIG, Hansson GV, Nicholls JM, Flodström SA (1982) Phys Rev Lett 48: 1032
19. (a) Perfetti P, Nicholls JM, Reihl B (1987) Phys Rev B 36: 6160; (b) Cricenti A, Selci S, Magnusson KO, Reihl B (1990) Phys Rev B 41: 12908
20. (a) Himpsel FJ, Heimann P, Eastman DE (1981) Phys Rev B 24: 2003; (b) Martensson P, Cricenti A, Hansson GV (1985) Phys Rev B 32: 6959
21. (a) Stroscio JA, Feenstra RM, Fein AP (1986) Phys Rev Lett 57: 2579; (b) Feenstra RM, Stroscio JA (1987) Phys Scr T19: 55
22. Feenstra RM (1999) Phys Rev B 60: 4478
23. Hansson GV, Uhrberg RIG (1988) Surf Sci Rep 9: 197
24. Cargnoni F, Gatti C, May E, Narducci D (2000) J Chem Phys 112: 887
25. Bader RFW (1990) Atoms in molecules: a quantum theory. International series of monographs on chemistry 22. Oxford University Press, Oxford
26. Bongiorno A, Colombo L, Cargnoni F, Gatti C, Rosati M (2000) Europhys Lett 50: 608
27. Cargnoni F, Gatti C, Colombo L (1998) Phys Rev B 57: 170
28. Cargnoni F, Colombo L, Gatti C (1997) Nucl Instrum Methods Phys Res B 127–128: 235
29. Saunders VR, Dovesi R, Roetti C, Causà M, Harrison NM, Orlando R, Zicovich-Wilson CM (1998) Crystal98, user's manual. University of Torino, Torino
30. Dirac PAM (1930) Proc Camb Philos Soc 26: 376
31. Becke AD (1993) J Chem Phys 98: 5648
32. (a) Perdew JP, Wang Y (1986) Phys Rev B 33: 8800; (b) Perdew JP, Wang Y (1989) Phys Rev B 40: 3399; (c) Perdew JP, Wang Y (1992) Phys Rev B 45: 13244
33. Hehre WJ, Radom L, Schleyer PvR, Pople JA (1986) Ab initio molecular orbital theory. Wiley, New York
34. Weast RC, Astle MJ, Beyer WH (1987) Handbook of chemistry and physics 67th edn. CRC, West Palm Beach, Fla
35. Pisani C (1996) In: Pisani C (ed) Quantum mechanical ab-initio calculation of the properties of crystalline materials. Lecture notes in chemistry 67. Springer, Berlin Heidelberg New York, pp 227–244
36. Keating PN (1966) Phys Rev 145: 637
37. Himpsel FJ, Batra IP (1984) J Vac Sci Technol A 2: 952

38. Ihm J, Zunger A, Cohen ML (1979) J Phys C 12: 4401, and references therein
39. Schwinger J (1951) Phys Rev 82: 914
40. Bader RFW (1994) Phys Rev B 49: 13348
41. Srebrenik S, Bader RFW, Nguyen-Dang TT (1978) J Chem Phys 68: 3667
42. Bader RFW, Carroll MT, Cheeseman JR, Chang C (1987) J Am Chem Soc 109: 7968
43. Bader RFW, Preston HJT (1970) Theor Chim Acta 17: 384
44. Bader RFW (1998) J Phys Chem 102: 7314
45. Bader RFW, Essen H (1984) J Chem Phys 80: 1943
46. Cheeseman JR, Carroll MT, Bader RFW (1988) Chem Phys Lett 143: 450
47. Bader RFW, MacDougall PJ, Lau CDH (1984) J Am Chem Soc 106: 1594
48. Lewis GN (1916) J Am Chem Soc 38: 762
49. Bader RFW, Heard GL (1999) J Chem Phys 111: 8789
50. MacDougall PJ, Bader RFW (1986) Can J Chem 64: 1496
51. Gatti C, MacDougall PJ, Bader RFW (1988) J Chem Phys 88: 3792
52. (a) Gatti C, Saunders VR, Roetti C (1994) J Chem Phys 101: 10686; (b) Gatti C (1996) Acta Crystallogr A 52: C555; (c) Gatti C, Cargnoni F (1997) III Convegno Nazionale di Informatica Chimica, Naples, Italy, pp 125–128 extended abstracts
53. Gatti C (1999) TOPOND98 user's manual. CNR-CSRSRC, Milan
54. Lee KH, Causà M, Park SS (1998) J Phys Chem 102: 6020
55. Tersoff J, Hamann DR (1985) Phys Rev B 31: 805
56. (a) Pisani C, Dovesi R. Roetti C (1988) In: Berthier G, Dewar MJS, Fischer H, Fukui K, Hall GG, Hinze J, Jaffé HH, Jortner J, Kutzelnigg W, Ruedenberg K, Tomasi J (eds) Hartree–Fock ab initio treatment of crystalline systems. Lecture notes in chemistry 48. Springer, Berlin Heidelberg New York, pp 28–33 and 144–149; (b) (1996) In: Pisani C (ed) Quantum mechanical ab-initio calculation of the properties of crystalline materials. Lecture notes in chemistry 67. Springer, Berlin Heidelberg New York, pp 40, 58
57. Koopmans TA (1933) Physica 1: 104
58. Aschroft NW, Mermin ND (1976) Solid state physics international edition. Saunders College, Philadelphia, pp 353–371
59. Cargnoni F (2000) Phd Thesis, University of Milano, Italy
60 Bayles D (2000) Phd Thesis, McMaster University, Hamilton, Ontario, Canada